Batteries & Supercaps

Research Article
doi.org/10.1002/batt.202500444

Chemistry Europe
European Chemical Societies Publishing

www.batteries-supercaps.org

Extended Cycle Life in Lithium-Ion Batteries through Lithium Supplementation from $Li_2C_4O_4$@SiO_2 Microcapsules

Bhupender Pal, Luka Jurečič, Matej Gabrijelčič, and Robert Dominko*

The formation of a solid electrolyte interphase (SEI) in lithium-ion batteries consumes active lithium ions, resulting in loss of capacity and decreased cycle life. Most prelithiation methods only address the initial lithium depletion by compensating with a source of lithium ions, overlooking the ongoing lithium consumption through continuous degradation processes. In this study, $Li_2C_4O_4$@SiO_2 microcapsules are presented, in which $Li_2C_4O_4$ serves as an additional source of lithium ions and the porous SiO_2 shell prevents unwanted catalytic reactions, ensuring sustained lithium availability throughout the cycling. The microcapsules are synthesized using a wet impregnation method and characterized using various techniques to confirm their structural, morphological, and compositional properties. Ex situ nuclear magnetic resonance (NMR) analysis demonstrated lithium-ion mobility, and electrochemical tests in full-cell configurations with graphite and graphite/silicon anodes confirmed improved capacity retention and cycle life. This work highlights the potential of microencapsulated lithium-ion sources to improve battery performance in various lithium-ion systems and opens a pathway for battery cells with self-healing functionality that can be triggered on demand.

1. Introduction

Lithium-ion batteries (LIBs) with longer cycle lives and higher energy density are in high demand. The functional principle of LIBs is based on the reversible exchange of lithium between two host structures, which theoretically enables an infinite lifetime. However, uncontrolled parasitic reactions that occur sporadically during lithium exchange degrade LIBs,[1,2] particularly during the formation cycle(s) when electrolyte and impurities on the surface of the composite electrodes are electrochemically decomposed. This process consumes and depletes lithium to a considerable extent and is negligible if the cell reaches thermodynamic equilibrium through passivation and thus prevents further decomposition.[3,4] The loss of lithium reduces the reservoir of reversibly transferable Li^+ ions between the anode and cathode, which subsequently affects the energy and power densities as well as the cycle life.[5] For high capacity anode materials such as Si, SiOx, and Sn, the initial loss of active lithium is greater (≈20–45%) than for graphite anodes (≈7–14%)[6,7] The dynamic nature of passive films leads to restructuring and additional depletion of active components. Furthermore, as the cells do not operate in ideal environments, further depletion of the lithium ions occurs through irreversible reactions. Consequently, active lithium ions may also be depleted during cycling, resulting in lower Coulombic efficiency (<100%).[8] In this context, the integration of pre-lithiation additives into cathode materials during the electrode manufacturing process is considered an effective strategy to solve the problem of initial loss of active lithium.[9,10] The ideal prelithiation additives are electrochemically active within the working potential of the cathode, possess high volumetric and gravimetric capacity, and compensate for lithium loss through passivation and other irreversible reactions.[11] Various lithium compounds such as LiN_3,[12] Li_3N,[13] Li_2S,[14] Li_2O,[15] Li_2NiO_2,[16] Li_2MoO_3,[17] and Li_2O_2,[18] have been proposed as pre-lithiation cathode additives; however, most of these additives are not compatible with standard cathode processing protocols and are unstable under ambient conditions. To mitigate the problem of active lithium loss and increase the energy density of current LIBs, a promising approach is to implement a lithium replenishment strategy by storing an additional amount of lightweight lithium carriers in the electrode composite. Therefore, it is more advantageous to use additives that are compatible with standard cathode processing protocols, stable under ambient conditions and cost-effective.

In this context, organic lithium salts such as dilithium squarate ($Li_2C_4O_4$) and lithium oxalate ($Li_2C_2O_4$) are recognized for their stability in the ambient atmosphere.[19,20] $Li_2C_4O_4$ has been used as a prelithiation agent in lithium-ion capacitors (LICs) and LIBs due to

B. Pal, L. Jurečič, M. Gabrijelčič, R. Dominko
Department of Materials Chemistry
National Institute of Chemistry
Hajdrihova 19, 1000 Ljubljana, Slovenia
E-mail: robert.dominko@ki.si

L. Jurečič, R. Dominko
Faculty of Chemistry and Chemical Technology
University of Ljubljana
Večna pot 113, 1001 Ljubljana, Slovenia

R. Dominko
Alistore-European Research Institute, CNRS FR 3104
80039 Amiens, France

Supporting information for this article is available on the WWW under https://doi.org/10.1002/batt.202500444

its balance between high gravimetric capacity (≈425 mAh g^{-1}) and low decomposition potential (≈3.6–4.2 V vs Li^+/Li).[21,22] $Li_2C_4O_4$ is considered a safe, easy to synthesize, low-cost, and air-stable additive for the prelithiation of LICs and LIBs[23] It has been combined with cathode materials in LICs such as activated carbon and in LIBs such as NMC, $LiPF_6$, $TiSb_2$, and Si-graphite.[24–26] Due to its easy processability with solvents such as *N*-methyl-2-pyrrolidone (NMP), $Li_2C_4O_4$ overcomes the main disadvantages of using Li_2S and Li_3N as prelithiation additives. Due to the easy processability of $Li_2C_4O_4$ in cathode materials, rapid scale-up of fabricated cells and electrodes is possible. It has also been reported that the use of $Li_2C_4O_4$ as a prelithiation additive not only functionalizes the electrode surface but also modifies the SEI itself.[23] Currently, it has been found that the use of $Li_2C_4O_4$ as a prelithiation additive increases the amount of organic species such as C═O, O═C—O and C—O and decreases the content of alkoxides and carbonates formed after solvent reduction.[23] The decomposition by-products (CO and CO_2) of $Li_2C_4O_4$ react with the electrolyte at the negative electrode surface at the Li-ion reduction potential and act as film-forming additives. The passivation layer formed contains a lower amount of Li and O but a higher amount of carbon, indicating a limited decomposition of the solvent for passive film formation. These results open up the possibility of using $Li_2C_4O_4$ not only as an additive for prelithiation but also as a film-forming additive for SEI to optimize the SEI of the negative electrode. However, besides all these advantages of $Li_2C_4O_4$ as an additive for prelithiation, there are also some disadvantages, such as gaseous products (CO and CO_2) during the decomposition of $Li_2C_4O_4$ and undesirable catalytic reactions when mixed with cathode materials (especially transition metals), which in turn can affect the structure of the original electrodes and significantly change the electrochemical performance of the device.[24,25]

We have opted for microcapsules that contain an additional source of lithium ions to avoid these potential side effects of $Li_2C_4O_4$. Microencapsulation is an innovative technique for preserving, protecting, and releasing active ingredients in various industrial applications such as pharmaceuticals, food, cosmetics, agrochemicals, detergents, and paints.[27,28] When developing microcapsule systems and their production processes, it is crucial to consider the environmental impact and energy costs of manufacturing. Currently, factors related to the EU's sustainability goals are changing the design direction of such microcapsule systems. A porous SiO_2-based material that is thermochemically stable, cost effective, safe, environmentally friendly, and abundant is an excellent choice for microcapsule structures.

In this work, we demonstrate an application of SiO_2-based microcapsules filled with $Li_2C_4O_4$. A three-step synthesis route was developed that leads to a homogeneous distribution of $Li_2C_4O_4$ in the capsules. $Li_2C_4O_4$ encapsulated in the porous SiO_2 microcapsule ($Li_2C_4O_4$@SiO_2) can be activated by electrochemical stimuli at a voltage higher than 4.2 V. The released lithium ions are ionic in character, as demonstrated by solid-state nuclear magnetic resonance (NMR). The advantage of adding $Li_2C_4O_4$@SiO_2 to the cathode composite with NMC622 active materials was demonstrated in full cell battery tests with graphite and silicon-graphite-based anodes.

2. Results and Discussions

The encapsulation of $Li_2C_4O_4$ in porous SiO_2 microcapsules was carried out using a wet impregnation method comprising three main steps, as illustrated in Scheme S1, Supporting Information. In the first step, porous SiO_2 microcapsules were synthesized by the hydrolysis and condensation of TEOS using ammonia as a catalyst. In the second step, $Li_2C_4O_4$ was synthesized by a simple wet chemical method using squaric acid (3,4-dihydroxy-3-cyclobutene-1,2-dione) and lithium carbonate as precursors. Finally, in the third step, the encapsulation of $Li_2C_4O_4$ into the porous SiO_2 microcapsules was carried out using the wet impregnation technique. The $Li_2C_4O_4$ loading in the porous SiO_2 microcapsules was optimized by varying the weight ratio of $Li_2C_4O_4$ in the SiO_2/$Li_2C_4O_4$ mixture from 1 to 25 wt%. **Figure 1** shows the XRD and FTIR characterizations of the microcapsules containing different proportions of $Li_2C_4O_4$. Both techniques show that up to 10 wt% of $Li_2C_4O_4$ can be successfully encapsulated in the microcapsules synthesized by this three-step process.

The XRD patterns of all samples are shown in Figure 1a. With increasing $Li_2C_4O_4$ content, the gradual formation of a crystalline phase is observed. A broad peak at about $2\theta = 23°$ corresponds to the amorphous nature of SiO_2. The main characteristic peaks of $Li_2C_4O_4$ indicate a monoclinic phase (space group C2/m), which is consistent with the crystalline $Li_2C_4O_4$ phase (PDF #04-012-0316). At a loading of up to 10 wt%, $Li_2C_4O_4$ remains in an amorphous state, probably due to the spatial confinement within the microcapsules. However, increasing the loading beyond 10 wt% results in the appearance of crystalline $Li_2C_4O_4$, indicating that excess material crystallizes outside the porous framework. Additional information was obtained from the FTIR analysis (Figure 1b), which supports the XRD results. The FTIR spectrum of porous SiO_2 shows three characteristic vibrational bands: asymmetric stretching at 1092 cm^{-1}, symmetric stretching at 800 cm^{-1}, and bending vibrations of Si–O–Si at 465 cm^{-1}. Additional bands around 1700 and 3430 cm^{-1} correspond to carboxyl and hydroxyl groups, respectively. A peak at 947 cm^{-1} is due to the Si–O stretching vibration of Si–OH. In the case of pure $Li_2C_4O_4$, a strong absorption band at 1550 cm^{-1} is observed, corresponding to the stretching vibrations of C═C and C═O bonds, while a band at 1100 cm^{-1} is attributed to C—C stretching. The absence of C–O vibrational bands in the FTIR spectrum indicates that $Li_2C_4O_4$ consists of two Li^+ ions and a squarate oxocarbon dianion ($C_4O_4^{2-}$) with four C═O and C—C bonds. In the composite microcapsules, the 1550 cm^{-1} band becomes increasingly clear with higher $Li_2C_4O_4$ content, confirming the successful incorporation of $Li_2C_4O_4$ into the SiO_2 framework. The intensity of the $Li_2C_4O_4$-related peaks increases proportionally with the $Li_2C_4O_4$/SiO_2 ratio. Although a complete optimization of the $Li_2C_4O_4$@SiO_2 synthesis process has not yet been achieved, the obtained material shows effective encapsulation of the sacrificial salt in porous silica spheres.

Research Article
doi.org/10.1002/batt.202500444
Chemistry Europe
European Chemical Societies Publishing

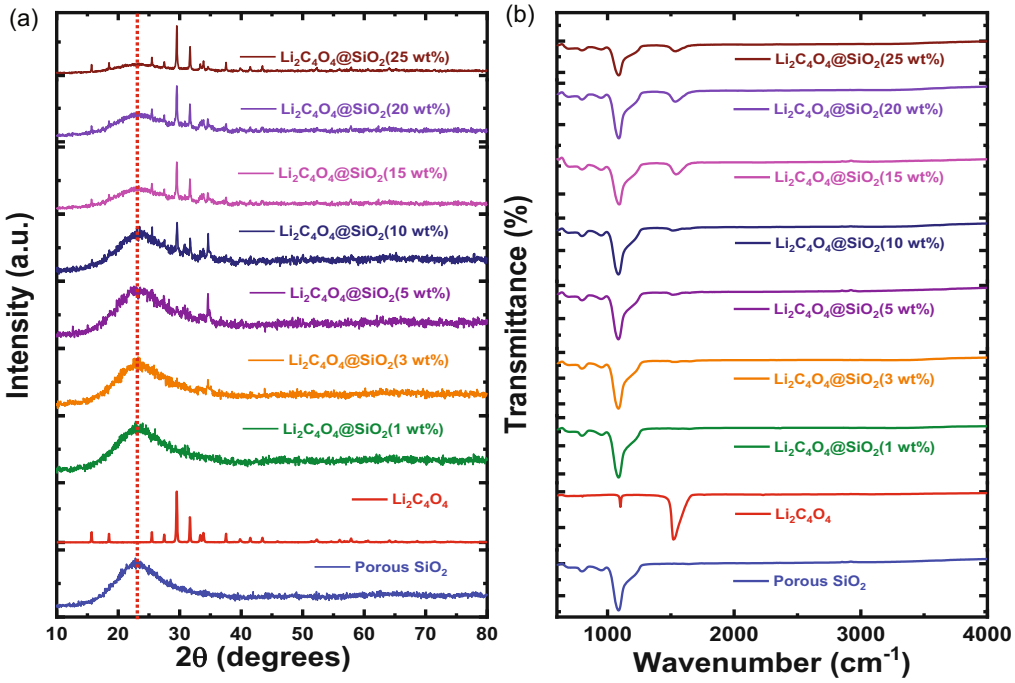

Figure 1. a) Powder X-ray diffraction patterns and b) FT-IR spectrum of as-synthesized porous SiO_2 shell, $Li_2C_4O_4$, and microcapsules ($Li_2C_4O_4$@SiO_2).

The microscopy images of the porous SiO_2 spheres, $Li_2C_4O_4$, and $Li_2C_4O_4$@SiO_2 microcapsules are shown in **Figure 2**. SEM images of the porous SiO_2 shells show a spherical morphology with diameters of 100–400 nm (Figure 2a). In contrast, the SEM images of pure $Li_2C_4O_4$ show rectangular and triangular structures with dimensions in the micrometer range (Figure 2b). Further SEM images of the $Li_2C_4O_4$@SiO_2 microcapsules can be found in Figure 2c,d. At low $Li_2C_4O_4$ loadings, the microcapsules retain the appearance of the original porous SiO_2 spheres. However, at higher loading (25 wt%), distinct crystalline $Li_2C_4O_4$ particles are observed next to the $Li_2C_4O_4$@SiO_2 microcapsules. Overall, the structural integrity of the SiO_2 spheres is preserved after infiltration with the $Li_2C_4O_4$ salt. Additional SEM images showing different $Li_2C_4O_4$ concentrations (1–25 wt%) within the porous SiO_2 microcapsules can be found in the Supporting Information (Figure S1, Supporting Information). To further confirm the core–shell structure of the $Li_2C_4O_4$@SiO_2 microcapsules, a TEM analysis of the porous SiO_2 spheres (Figure 2e) and the $Li_2C_4O_4$@SiO_2 microcapsules (Figure 2f,g) was performed. A clear contrast between the two images demonstrates the presence of $Li_2C_4O_4$ within the porous SiO_2 structure (see Figure 2g for a higher magnification view). Further TEM images demonstrating the successful formation of $Li_2C_4O_4$@SiO_2 microcapsules can be found in the Supporting Information (Figure S1, Supporting Information). The TEM images confirm the porous, microcapsule-like structure with a shell thickness of about 50–65 nm and the successful encapsulation of $Li_2C_4O_4$. However, not all microcapsules appear to be completely filled with $Li_2C_4O_4$, indicating that there is potential for further optimization of the encapsulation process. Elemental mapping of the microcapsules was performed and shows the presence of Si, O, and C, as shown in Figure S1(B), Supporting Information.

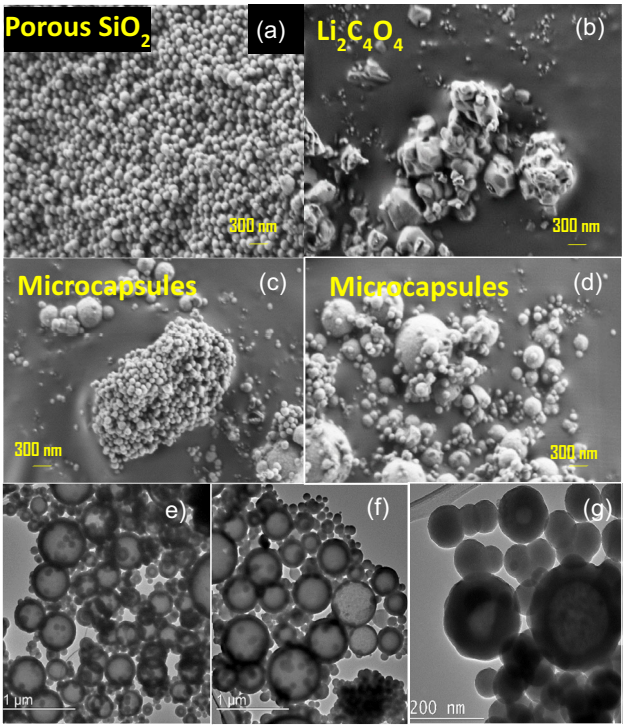

Figure 2. Scanning electron microscopy images (SEM) showing porous SiO_2 shells a), lithium squarate b), microcapsules ($Li_2C_4O_4$@SiO_2) in frames c,d). Transition electron microscopy (TEM) images of porous SiO_2 e) and microcapsules ($Li_2C_4O_4$@SiO_2) at two different magnifications f,g).

X-ray photoelectron spectroscopy (XPS) was used to analyze the elemental composition and chemical bonding states in SiO_2, $Li_2C_4O_4$, and the $Li_2C_4O_4$@SiO_2 microcapsules. The materials

Research Article
doi.org/10.1002/batt.202500444
Chemistry Europe
European Chemical Societies Publishing

consist mainly of silicon, oxygen, lithium, and carbon. Spectral fitting was performed to obtain detailed information on the distribution and relative abundance of the elements. In the XPS wide-scan spectra of SiO_2, $Li_2C_4O_4$, and $Li_2C_4O_4$@SiO_2 microcapsules, peaks corresponding to Si, O, C, and Li were observed, as shown in Figure S2, Supporting Information. For SiO_2, the XPS core level spectra of Si 2*p*, O 1*s* and C 1*s* are shown in **Figure 3**a–c. A single peak at 103.2 eV in the Si 2*p* spectrum and a peak at 533.1 eV in the O 1*s* spectrum correspond to the typical binding energies of Si—O bonds in amorphous SiO_2. For pure $Li_2C_4O_4$ (Figure 3d–f), the Li 1*s* peak appears at 56.1 eV, characteristic of Li–O bonding. The C 1*s* spectrum is deconvoluted into three peaks at 284.6, 286.2 and 288.6 eV, which are assigned to C—C, C—O, and O═C—O bonds, respectively—in agreement with the functional groups in lithium squarate and confirmed by the IR spectroscopy results. The O 1*s* spectrum shows two peaks at 533.0 and 533.3 eV, which are attributed to the C═C and O—C bonding states, respectively. In the case of $Li_2C_4O_4$@SiO_2 microcapsules (Figure 3d–f), the fitted peaks for Si 2*p*, O 1*s* and C 1*s* closely resemble those observed in the individual components. A slight deviation is observed in the O 1*s* spectrum, which shows a splitting into three peaks corresponding to Si—O, C—O, and O═C—O bonds. This spectral feature confirms the coexistence of SiO_2 and $Li_2C_4O_4$ bonds. Overall, the presence of all characteristic peaks confirms the successful encapsulation of $Li_2C_4O_4$ within the porous SiO_2 microcapsules.

We used solid-state NMR to investigate the ionic character of lithium after the decomposition of $Li_2C_4O_4$. The tests were carried out in environments with sodium metal and electrodes consisting of either $Li_2C_4O_4$ powder or $Li_2C_4O_4$@SiO_2 microcapsules. The ionic character of lithium after decomposition was determined in two different environments using carbonate-based electrolytes with $NaPF_6$ salt (NP30 electrolyte) or $LiPF_6$ salt (LP57 electrolyte). Schematic representations of the Swagelok cell used for the

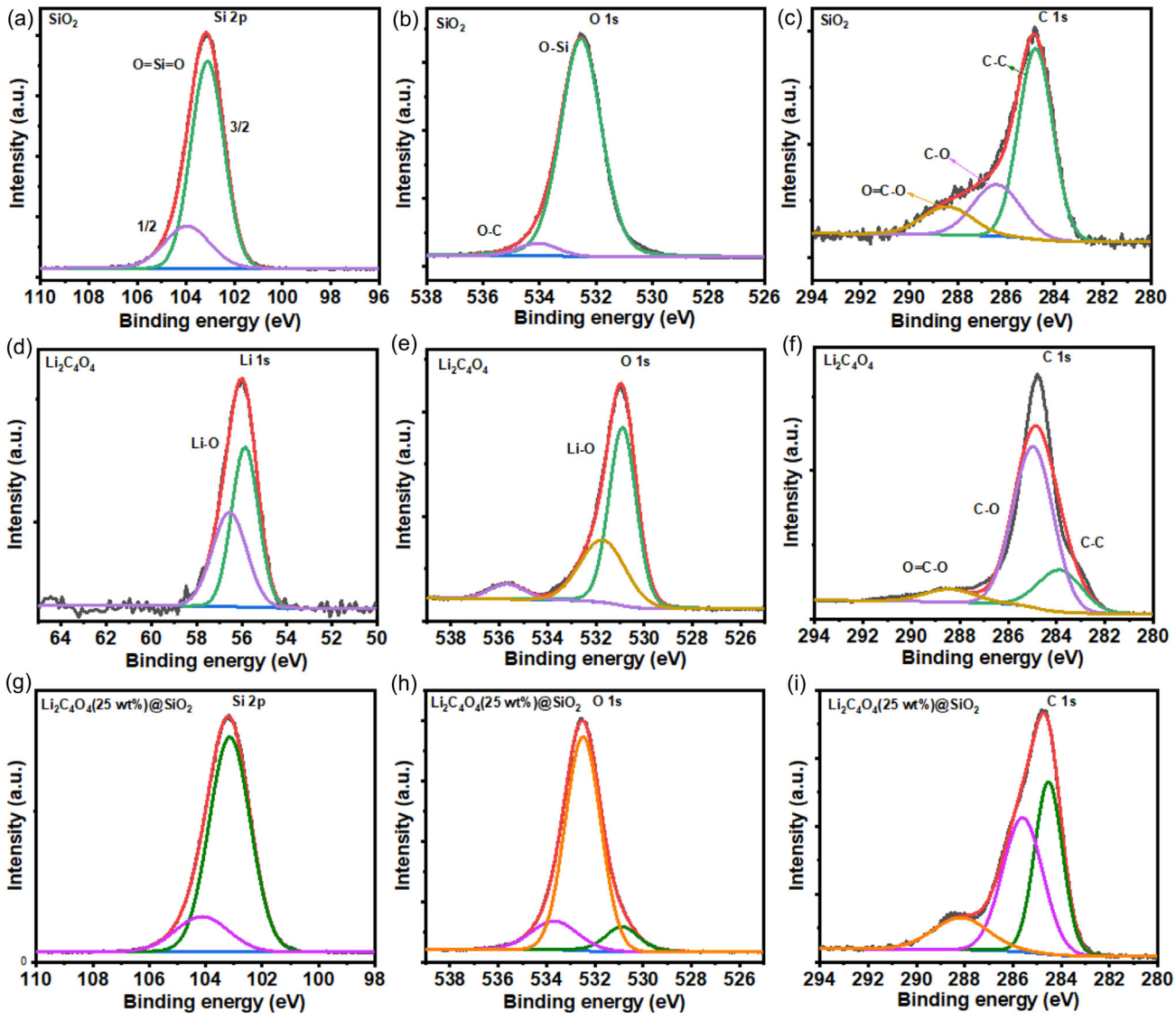

Figure 3. XPS spectra of porous SiO_2, $Li_2C_4O_4$, and microcapsules ($Li_2C_4O_4$@SiO_2) a–i). Si 2*p*, O 1*s*, Li 1*s*, and C 1*s*.

Research Article
doi.org/10.1002/batt.202500444
Chemistry Europe
European Chemical Societies Publishing

electrochemical studies and the MAS rotor used for the ex situ NMR analysis are shown in Figure S3a,b, Supporting Information. First, the $Li_2C_4O_4$ powder and $Li_2C_4O_4$@SiO_2 microcapsules were pressed into pellets. These pellets were assembled in Swagelok cells with a glass fiber separator, the two different electrolytes (NP30 or LP57) and a sodium metal sheet as a counter electrode. The cells were charged from 2.5 to 4.4 V at a constant current with a C-rate of C/50, followed by an 8-h rest period. After cycling, the Swagelok cells were transferred to an argon-filled glovebox and the cycled powder ($Li_2C_4O_4$ or $Li_2C_4O_4$@SiO_2) was collected and loaded into MAS rotors for further ex-situ NMR measurements. The combined NMR spectra are shown in **Figure 4**a, where a slight shift in the Li^+ ion peaks can be observed, likely due to changes in the local chemical environment after cycling. Figure 4b compares the NMR spectra of bare $Li_2C_4O_4$ and cycled Na metal//$Li_2C_4O_4$ in NP30 and LP57 electrolytes. The results show a broad signal centered between 5 and −5 ppm for the pristine $Li_2C_4O_4$ powder. In contrast, the cycled samples exhibit an additional sharp peak, confirming the presence and mobility of Li^+ ions after the decomposition of $Li_2C_4O_4$. The intensity of this sharp signal is significantly higher in the LP57 electrolyte, which can be attributed to the presence of Li^+ ions from $LiPF_6$. Similarly, the $Li_2C_4O_4$@SiO_2 microcapsules also show a sharp NMR signal with a slight shift, as shown in Figure 4c. These results, obtained in two different battery configurations, confirm the ionic nature of the lithium released by the decomposition of $Li_2C_4O_4$.

Next, we assembled several battery cells to evaluate the effects of microcapsules in a full cell configuration with a graphite anode. The microcapsules were incorporated into the cathode, which consisted of the active material NMC622. A schematic representation of the experimental setup can be found in the *Supplementary Information* (Scheme S2, Supporting Information). Cyclic voltammetry (CV) scans of graphite//NMC622 full cells in LP57 electrolyte were performed between 2.5 and 4.5 V at a scan rate of 0.1 mV s^{-1},

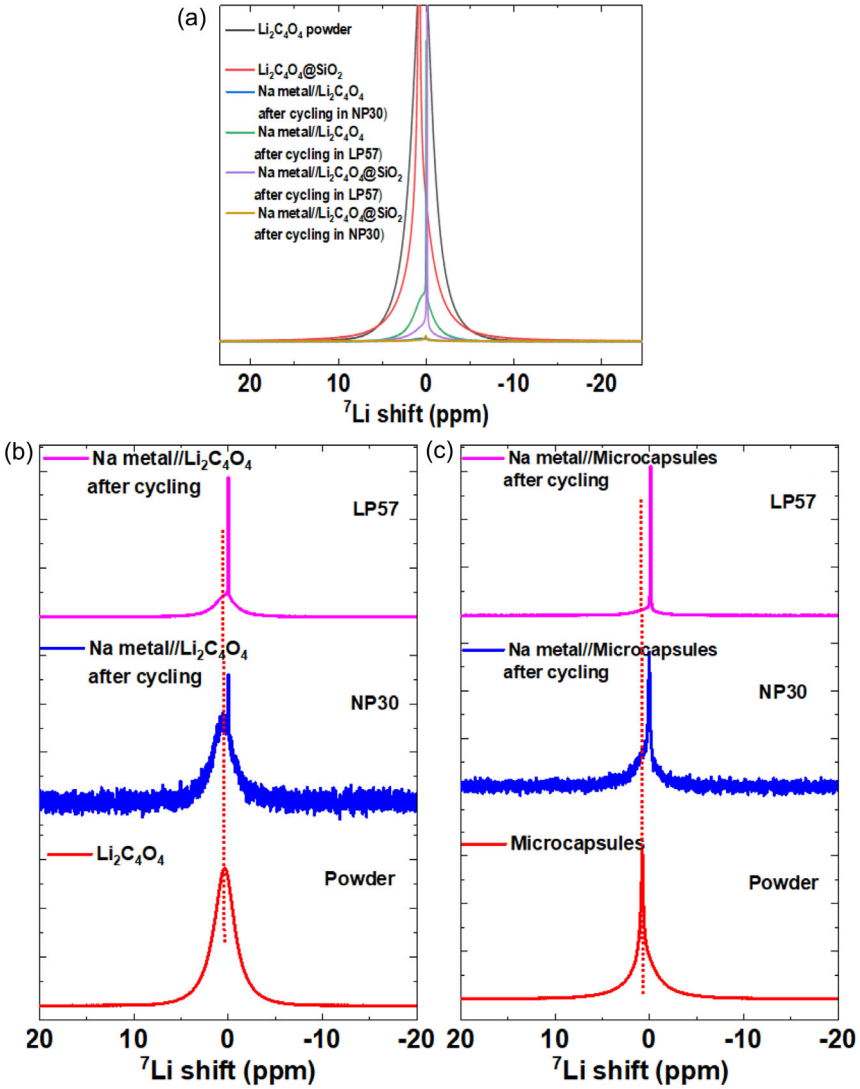

Figure 4. a–c) Solid-state ^7Li NMR spectra of $Li_2C_4O_4$, microcapsules and cycled half-cells (Na metal//$Li_2C_4O_4$ and Na metal//microcapsules) in NP30 and LP57 electrolytes.

Research Article
doi.org/10.1002/batt.202500444
Chemistry Europe
European Chemical Societies Publishing

both with and without microcapsules, as shown in **Figure 5**a,b. The CV scan of the cell without $Li_2C_4O_4@SiO_2$ microcapsules (Figure 5a) shows typical oxidation/reduction peaks associated with the Ni^{2+}/Ni^{4+} redox transitions. In contrast, the cell with $Li_2C_4O_4@SiO_2$ microcapsules shows an additional oxidation peak at around 4.2 V, which corresponds to the irreversible oxidation of $Li_2C_4O_4$ and confirms the release of Li^+ ions from the microcapsules (Figure 5b). CV and galvanostatic charge/discharge curves for different weight percentages of $Li_2C_4O_4$ in the microcapsules are shown in the Supporting Information (Figure S4a,b, Supporting Information). The addition of $Li_2C_4O_4@SiO_2$ microcapsules slightly increases the polarization during the first charging cycle (Figure S5a, Supporting Information), which is repeatable (Figure S5b, Supporting Information) and can probably be reduced by appropriate electrode engineering. The irreversible oxidation of $Li_2C_4O_4$ within the microcapsules releases additional Li^+ ions, which improve both the specific capacity and the stability of the cell. This was validated in full cells with graphite as the anode and NMC622 as the cathode material. The galvanostatic cycling data for pouch cells are shown and compared in Figure 5c. The initial capacity of the battery containing $Li_2C_4O_4@SiO_2$ microcapsules in the cathode is lower than that of the cell without microcapsules, which is probably due to the non-optimized cathode composite preparation. Battery cells containing $Li_2C_4O_4@SiO_2$ microcapsules show lower Coulombic efficiency during the formation cycle, which can be attributed to the decomposition of $Li_2C_4O_4$, consuming additional charge. While the capacity of the control cell (without microcapsules) stabilizes after the second cycle, the capacity of the cell with

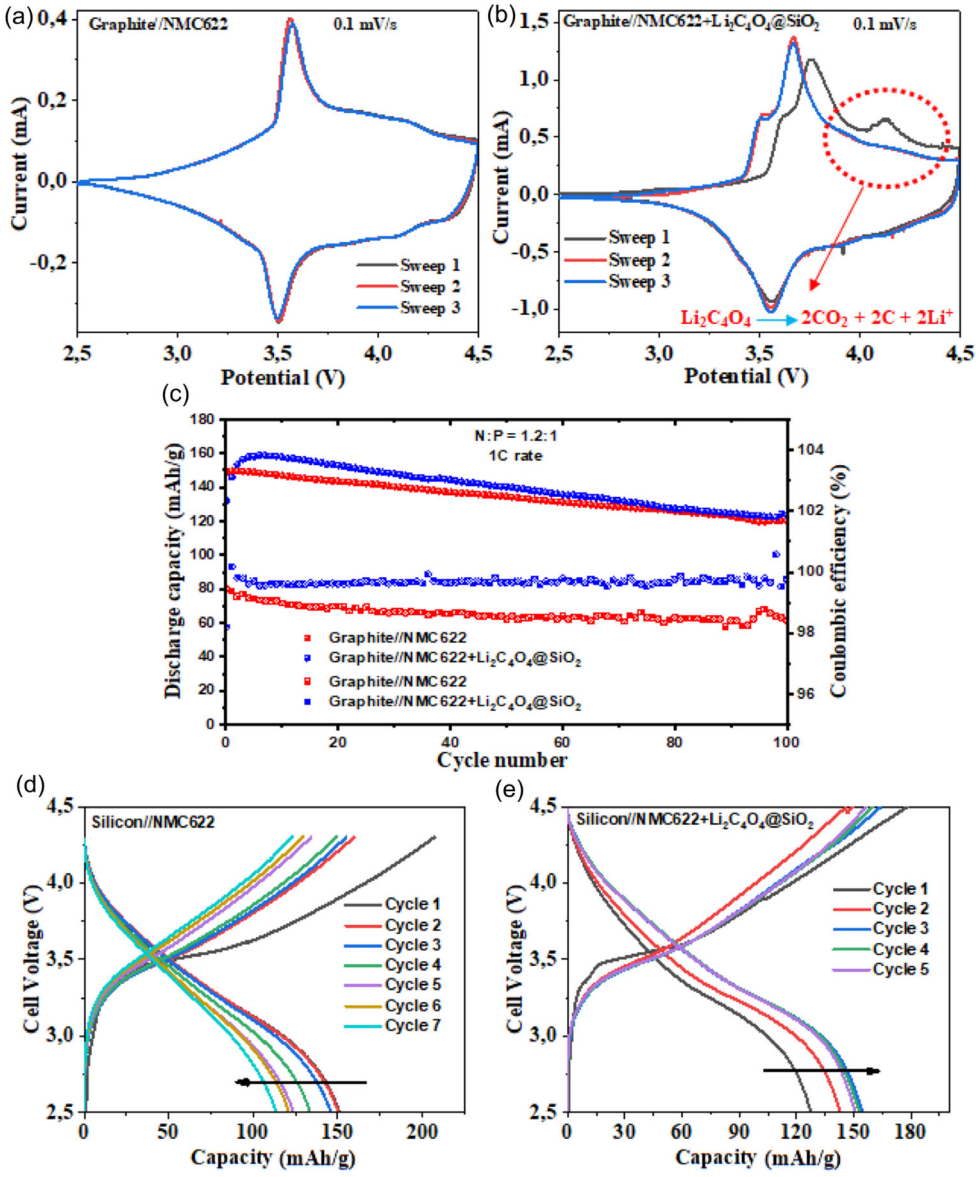

Figure 5. Electrochemical characterization of full cells. a,b) Cyclic voltammetry (CV) curves. c) cycling performance and coulombic efficiency of graphite// NMC622 full-cells without and with microcapsules in the voltage range of 2.5–4.5 V at a scan rate of 0.1 mV s^{-1} or at 1C rate in LP57 electrolyte. d,e) charge/discharge voltage profiles of silicon//NMC622 and silicon//NMC622 with microcapsules in the voltage range of 2.5–4.3 V at 1C rate in LP57 electrolyte.

microcapsules gradually increases and reaches a maximum value around the sixth or seventh cycle. This gradual increase is probably due to the slow diffusion of lithium ions from the microcapsules, further research is needed to understand the kinetics of lithium release. Nevertheless, the reversible capacity of the battery with microcapsules exceeds that of the control cell due to the higher lithium inventory available for exchange between the electrodes. The degradation products of dilithium squarate have been reported to positively influence the formation of cathode electrolyte interphase (CEI) and solid electrolyte interphase (SEI). We attribute the improved Coulombic efficiency in the cell with microcapsules to the formation of more stable passivation layers as a result of the decomposition of squarate anions. Although this decomposition initially increases the reversible capacity, further optimization of the electrode formulation is required to maintain the increased capacity during longer cycles.

Further galvanostatic measurements were carried out with silicon/graphite composite anodes in combination with NMC622 cathodes, both with and without $Li_2C_4O_4$@SiO_2 microcapsules in the cathode composite. Figure 5d,e compare the electrochemical performance of these battery cells. Similar to the graphite// NMC622 system, the battery with microcapsules shows an increase in reversible capacity during the first few cycles (Figure 5d). In contrast, the cell without microcapsules shows a rapid decrease in capacity due to the high silicon content in the anode (Figure 5e). Since the only difference between these cells is the presence of $Li_2C_4O_4$ stored in the microcapsules, the improved performance is attributed to the additional lithium released during $Li_2C_4O_4$ decay. Interestingly, the increase in capacity occurs gradually over several cycles, further supporting the controlled release mechanism.

3. Conclusions

We successfully synthesized $Li_2C_4O_4$@SiO_2 microcapsules by incorporating lithium squarate ($Li_2C_4O_4$) into porous SiO_2 spheres using a wet impregnation method. Our results show that this method is particularly effective at lower $Li_2C_4O_4$ concentrations (below 10 wt%), which helps to maintain the structural integrity of the core–shell microcapsules. Various characterization techniques confirmed the successful encapsulation of $Li_2C_4O_4$ within the porous SiO_2 matrix. The microcapsules were then used as a 2 wt% additive in a cathode composite containing NMC622 as active material. Cyclic voltammetry showed the characteristic reversible redox peaks of NMC622, together with an additional irreversible oxidation peak at about 4.2 V. This peak corresponds to the decomposition of $Li_2C_4O_4$ and the associated release of Li^+ ions into the electrolyte. The ionic nature of the released lithium was further confirmed by solid-state NMR in a controlled system with a sodium metal anode and a sodium-containing electrolyte, in which $Li_2C_4O_4$ was electrochemically decomposed.

Although lithium release from $Li_2C_4O_4$ occurs within the electrochemical window of NMC622, the additional lithium inventory contributes to improved reversible capacity in full-cell configurations using either graphite or graphite–silicon composite anodes. In both systems, a gradual increase in reversible capacity was observed over several cycles, indicating slow lithium diffusion from the SiO_2 spheres following squarate decomposition. Improved Coulombic efficiency was also observed in experiments with graphite-based anodes, likely due to the positive effects of the squarate decomposition products on the formation of the SEI or CEI.

This strategy could be further optimized by applying a controlled-release coating to the microcapsules. Such coatings, activated by temperature or high voltage, could enable the targeted release of lithium or other additive at specific points during the battery's life cycle, for example, when the cell reaches 80% of its initial capacity, offering a promising route toward extending battery performance and longevity.

4. Experimental Section

Materials

Tetraethoxysilane (TEOS), absolute ethanol (EtOH), ammonia solution (NH_4OH), sodium polyacrylate ($(C_3H_3NaO_2)_n$), 3,4-dihydroxy-3-cyclobutene-1,2-dione (squaric acid), lithium carbonate (Li_2CO_3), and deionized water were used as received.

Synthesis of Porous SiO_2 Microcapsules

Porous SiO_2 microcapsules were synthesized at room temperature by dissolving 0.08 g of sodium polyacrylate in 1.5 mL of ammonia solution and then adding 30 mL of EtOH, which turned the solution white. After 30 min, 0.75 mL TEOS was added to the solution at 2-h intervals with vigorous stirring. After 12 h of continuous stirring, white colloids were obtained. Finally, hollow porous SiO_2 microcapsules were prepared by removing the sodium polyacrylate by repeated washing with deionized water and drying overnight at 80 °C.

Synthesis of Dilithium Squarate ($Li_2C_4O_4$)

$Li_2C_4O_4$ was synthesized via a simple wet chemical method using squaric acid and lithium carbonate as starting materials. Squaric acid and Li_2CO_3 were dissolved in a 1:1 mixture of deionized water and EtOH at room temperature and stirred continuously for 4 h. The solvents were evaporated using a rotary evaporator at 50 °C. The resulting white powders were ground using a mortar and pestle and dried overnight under vacuum at 50 °C.

Encapsulation of $Li_2C_4O_4$ inside Porous SiO_2 Microcapsules ($Li_2C_4O_4$@SiO_2)

$Li_2C_4O_4$@SiO_2 microcapsules were synthesized using a wet impregnation method as shown in Scheme S1, Supporting Information. The $Li_2C_4O_4$ content within the SiO_2 microcapsules was optimized by varying the concentration from 1 to 25 wt%. A solution of $Li_2C_4O_4$ in water was added dropwise to the dry SiO_2 powder (1 mL g^{-1}) until it was completely wetted, and then left for almost 6 h to complete the impregnation of $Li_2C_4O_4$ in the porous SiO_2 microcapsules. Subsequently, the water was removed by drying at 80 °C overnight, followed by vacuum drying at 50 °C to recrystallize $Li_2C_4O_4$ within the porous SiO_2 microcapsules.

Material Characterization

The synthesized materials were characterized for their structural, compositional and morphological features using various techniques. Phase purity and crystal structure were examined using a PANalytical X'Pert PRO X-ray powder diffractometer (Cu Kα_1 radiation, $\lambda = 1.5406$ Å). The functional groups were identified using Fourier transform infrared spectroscopy (FT-IR) with a PerkinElmer Frontier spectrometer. The surface morphology was analyzed by SEM and TEM. SEM analysis was performed using a field emission SEM (Apreo 2 S, Thermo Fisher Scientific, Netherlands) equipped with a Clean Connect vacuum transfer system and an energy dispersive spectrometer (EDS). TEM analysis was performed on samples dispersed in acetone and placed on a TEM grid using the TEM, JEM-ARM200CF. X-ray photoelectron spectroscopy (XPS) was performed using a PHI Versa Probe III AD (Physical Electronics, USA) with a monochromatic Al Kα X-ray source (1486.6 eV); binding energies were referenced to the Au standard (Au 4f = 83.99 eV) and analyzed using MultiPak software.

Electrode Preparation, Cell Assembly, and Electrochemical Testing

The cathode composites were prepared by slurry casting, as shown in Scheme S2, Supporting Information. For Li-metal//$Li_2C_4O_4$ and Li-metal//microcapsule half cells, the positive electrode consisted of 70 wt% active material ($Li_2C_4O_4$ or microcapsules), 15 wt% carbon black (conductive agent) and 15 wt% PVDF (binder) in *N*-methyl-2-pyrrolidone (NMP, solvent). For Li-metal//NMC622 + microcapsules half-cells and graphite//NMC622 + microcapsules full-cells, the positive electrode consisted of 88 wt% NMC622 (active material), 2 wt% microcapsules, 5 wt% carbon black and 5 wt% PVDF in NMP. Negative electrodes consisted of 85 wt% graphite, 5 wt% carbon black, 7.7 wt% CMC, and 2.3 wt% PAA in deionized water. The slurries were applied to Cu (negative) and Al (positive) foils using a line coater and dried overnight at 100–110 °C in a vacuum. The electrodes had a diameter of 18 mm (negative) and 16 mm (positive) and an N/P ratio of about 1.2:1. A single-layer Celgard 2500 separator (Ø = 20 mm) was used, which was impregnated with 60 µL LP57 electrolyte (1 M $LiPF_6$ in 3:7 vol% EC/EMC). The pouch cells were assembled in an Ar-filled glove box (O_2 and $H_2O < 0.1$ ppm). At least 2–3 cells per sample were prepared to ensure reproducibility. The effects of different contents of $Li_2C_4O_4$ (1–25 wt%) and microcapsules (1–2 wt%) in the cathode were systematically investigated. The electrochemical tests were performed at room temperature using Biologic VMP3 devices. Half and whole cells were cycled in a voltage range of 2.5–4.5 V at different C-rates (as indicated in the captions). Cyclic voltammetry (CV) was also performed using EC-lab at a scan rate of 0.1 mV s^{-1}. The mobility of Li^+ ions from the microcapsules was investigated by ex situ NMR measurements.

Sample Preparation and Ex-Situ NMR Measurements

To evaluate the mobility of Li^+ ions from microcapsules, ex-situ solid-state NMR was performed on powder samples assembled in Swagelok-type cells. Pristine $Li_2C_4O_4$ and $Li_2C_4O_4$@SiO_2 powders (≈20 mg each) were pressed into pellets, stacked with two glass fiber separators (GF-A) wetted with 150 µL of NP30 (1 M NaPF6 in 1:1 vol% EC:DMC) or LP57 electrolyte and paired with a Na-metal counter electrode. The cells were charged at C/50 from 2.5 to 4.4 V and rested for 8 h. After disassembly in the glove box, the cycled powders were collected and placed in magic angle spinning (MAS) rotors for NMR analysis. Solid-state MAS NMR spectra were recorded with a Bruker AVANCE NEO 400 MHz spectrometer using a 4 mm CP-MAS probe. 7Li MAS NMR was used to assess Li^+ mobility, with a Larmor frequency of 155.51 MHz and a MAS speed of 10 kHz. The spectra were recorded with an excitation pulse of 2.8 µs, 240 scans and a delay of 5 s between scans. The chemical shifts were referenced to adamantane, and the diamagnetic lithium species were identified based on the known shifts: Li_2O (≈2.8 ppm), $LiOH \times H_2O$ (≈0.4 ppm), Li_2CO_3 (0.0 ppm), and LiF (−1.0 ppm).

Acknowledgements

The authors acknowledge the financial support provided by the European Union's Horizon Europe research and innovation programme under Grant Agreement No. 101104028 (SALAMANDER) and the European Union's Horizon 2020 research and innovation program under Grant Agreement No. 101104022 (BATTERY 2030+ CSA3). The authors acknowledge the financial support from the Slovenian Research and Innovation Agency (research core funding No. P2-0423). The authors are grateful to Ms. Rabail Abbasi, dr. Elena Tchernychova, dr. Alen Vižintin (National Institute of Chemistry, Slovenia) and dr. Olivera Lužanin for helping with microscopy and XPS measurements.

Conflict of Interest

The authors declare no conflict of interest.

Data Availability Statement

The data that support the findings of this study are available from the corresponding author upon reasonable request.

Keywords: cathode additive · degradation · dilithium squarate · Li-ion batteries · lithiation additive · self-healing

[1] M. Li, J. Lu, Z. Chen, K. Amine, *Adv. Mater.* **2018**, *30*, 1800561.
[2] M. Armand, J. M. Tarascon, *Nature* **2008**, *451*, 652.
[3] R. Zhan, X. Wang, Z. Chen, Z. W. She, L. Wang, Y. Sun, *Adv. Energy Mater.* **2021**, *11*, 2101565.
[4] S. K. Heiskanen, J. Kim, B. L. Lucht, *Joule* **2019**, *3*, 2322.
[5] F. Holtstiege, A. Wilken, M. Winter, T. Placke, *Phys. Chem. Chem. Phys.* **2017**, *19*, 25905.
[6] Y. Jin, B. Zhu, Z. Lu, N. Liu, J. Zhu, *Adv. Energy Mater.* **2017**, *7*, 1700715.
[7] M. N. Obrovac, V. L. Chevrier, *Chem. Rev.* **2014**, *114*, 11444.
[8] A. J. Smith, J. C. Burns, S. Trussler, J. R. Dahn, *J. Electrochem. Soc.* **2009**, *157*, A196.
[9] Y. Sun, H. W. Lee, Z. W. Seh, N. Liu, J. Sun, Y. Li, Y. Cui, *Nat. Energy* **2016**, *1*, 1.
[10] P. Jezowski, O. Crosnier, E. Deunf, P. Poizot, F. Béguin, T. Brousse, *Nat. Mater.* **2018**, *17*, 167.
[11] F. Holtstiege, P. Bärmann, R. Nölle, M. Winter, T. Placke, *Batteries* **2018**, *4*, 4.
[12] D. Shanmukaraj, S. Grugeon, S. Laruelle, G. Douglade, J. M. Tarascon, M. Armand, *Electrochem. Commun.* **2012**, *12*, 1344.
[13] K. Park, B. C. Yu, J. B. Goodenough, *Adv. Energy Mater.* **2016**, *6*, 1502534.
[14] Y. Zhan, H. Yu, L. Ben, B. Liu, Y. Chen, Y. Wu, H. Li, W. Zhao, X. Huang, *J. Mater. Chem. A* **2018**, *6*, 6206.
[15] X. Hou, Y. Yang, Y. Mao, J. Song, J. Yang, G. Li, Y. Pan, Y. Wang, J. Xie, *J. Electrochem. Soc.* **2019**, *166*, A3387.
[16] H. Park, T. Yoon, Y. U. Kim, J. H. Ryu, S. M. Oh, *Electrochim. Acta* **2013**, *108*, 591.

[17] K. S. Park, D. Im, A. Benayad, A. Dylla, K. J. Stevenson, J. B. Goodenough, *Chem. Mater.* **2012**, *24*, 2673.
[18] L. Zhang, S. Jeong, N. Reinsma, K. Sun, D. S. Maxwell, P. Gionet, T. Yu, *J. Electrochem. Soc.* **2021**, *168*, 120520.
[19] B. Shen, B. Sarkodie, L. Zhang, H. Jiang, C. Li, Y. Hu, *Energy Storage Mater.* **2022**, *45*, 687.
[20] M. Arnaiz, D. Shanmukaraj, D. Carriazo, B. Bhattacharjya, A. Villaverde, M. Armand, J. A. Ajuria, *Energy Environ. Sci.* **2020**, *13*, 2441.
[21] G. Liu, W. Wan, Q. Nie, C. Zhang, X. Chen, W. Lin, X. Wei, Y. Huang, J. Li, C. Wang, *Energy Environ. Sci.* **2024**, *17*, 1163.
[22] A. G. Martin, M. M. Gnutzmann, E. Adhitama, L. Frankenstein, B. Heidrich, M. Winter, T. Placke, *Adv. Sci.* **2022**, *9*, 2201742.
[23] M. G. Moreno, R. Cid, M. Arnaiz, E. Goikolea, J. Ajuria, *ACS Appl. Mater. Interfaces* **2024**, *16*, 61846.
[24] M. Arnaiz, M. C. Rodríguez, D. Carriazo, A. Villaverde, J. Ajuria, *Electrochim. Acta* **2023**, *437*, 141456.
[25] M. Arnaiz, J. Ajuria, *J. Power Sources* **2021**, *515*, 230633.
[26] G. Lin, T. Meng, Y. Peng, P. Li, X. Hu, *Small Methods* **2025**, *9*, 2401133.
[27] B. T. Lobel, D. Baiocco, M. Al-Sharabi, A. R. Routh, Z. Zhang, O. J. Cayre, *ACS Appl. Mater. Interfaces* **2024**, *16*, 40326.
[28] C. Contini, W. Hu, W. Elani, *Chem. Commun.* **2022**, *58*, 4409.

Manuscript received: June 9, 2025
Revised manuscript received: July 29, 2025
Version of record online: